Performance of a hybrid direct ethylene glycol fuel cell

Z.F. Pan, B. Huang, L. An*

Department of Mechanical Engineering, The Hong Kong Polytechnic University, Hung Hom, Kowloon, Hong Kong SAR, China.

*Corresponding author.

Email: liang.an@polyu.edu.hk (L. An)

Abstract

In this work, a hybrid fuel cell is developed and tested, which is composed of an alkaline anode, an acid cathode, and a cation exchange membrane. In this fuel cell, ethylene glycol and hydrogen peroxide serve as fuel and oxidant, respectively. Theoretically, this fuel cell exhibits a theoretical voltage reaching 2.47 V, whereas it is experimentally demonstrated that the hybrid fuel cell delivers an open-circuit voltage of 1.41 V at 60°C. More impressively, this fuel cell yields a peak power density of 80.9 mW cm^{-2} (115.3 mW cm^{-2} at 80°C). Comparing to an open-circuit voltage of 0.86 V and a peak power density of 67 mW cm^{-2} previously achieved by a direct ethylene glycol fuel cell operating with oxygen, this hybrid direct ethylene glycol fuel cell boosts the open-circuit voltage by 62.1% and the peak power density by 20.8%. This significant improvement is mainly attributed not only to the high-voltage output of this hybrid system design, but also to the faster kinetics rendered by the reduction reaction of hydrogen peroxide.

Keywords: Fuel cells; Direct ethylene glycol fuel cell; Hydrogen peroxide; Operation parameters; Power density

1. Introduction

Fuel cells, which are alternative choices for power supply sources, have attracted extensive research interest due to its potential to be an efficient and clean energy conversion technology [1-8]. Currently, hydrogen, methanol, ethanol, and formate are four of the most common fuels utilized in fuel cells [9-15]. Among them, the source, transport, and storage of hydrogen are still remaining to be solved for widespread application. In addition, since the gaseous hydrogen has to be compressed into liquid phase to reduce the device volume, the high pressure may lead to a potential safety problem [16]. As for methanol, severe fuel crossover can result in dramatic performance degradation [17]. As for ethanol, the C-C bond is hardly broken in fuel cells running at low temperatures (generally < 60°C), leading to a low electron transfer rate (i.e., 33%) [16, 18]. Ethylene glycol (EG), an alternative choice for fuel, has received considerable interest for mobile, stationary, and portable applications, resulting from its promising theoretical energy capacity of 4.8 Ah mL^{-1}, high boiling point of 198°C, and outstanding efficiency of electric power conversion [19]. Hence, the use of liquid EG not only avoids the poisoning and safety problems, but also possesses an electron transfer rate as high as 80% [20].

On the cathode, pure oxygen and air are used as oxidant in most cases [20, 21]. On one hand, the pure oxygen needs to be compressed and stored in a tank particularly, which not only makes the fuel cell system bulkier, but also increases the system design complexity. On the other hand, ambient environment can provide adequate air to sustain the fuel cell operation, which makes the fuel cell system more compact and cost-effective [22]. Hence, the utilization of the air in fuel cells is more attractive. Although promising, one major issue impeding the commercialization of this fuel cell running on the air is the carbonate issue in alkaline fuel cells, which refers to the behavior that CO_2 in the air reacts with OH^- to form carbonate [1]. Two undesired phenomena

will occur when the carbonate is formed. One is that the carbonate precipitation in the cathode may cover the active sites for the reaction, resulting in the sluggish oxygen reduction reaction (ORR) kinetics [23]. The other is that the pores and channels in the cathode may be blocked when the precipitation gets larger, which elevates the transport resistance of oxygen [24]. Recently, the use of hydrogen peroxide acting as oxidant to replace the air or pure oxygen has been extensively investigated [25, 26]. As the supply of air and oxygen are insufficient in special cases, e.g. outer space and underwater, the fuel cells running on hydrogen peroxide are still able to operate under these conditions. In addition, the use of liquid hydrogen peroxide provides the several advantages: (1) a substantial increase in the theoretical voltage; (2) low activation loss on the cathode due to two-electron transfer; and (3) negligible effects of water flooding issue [27].

In this work, a hybrid fuel cell running on ethylene glycol as fuel and hydrogen peroxide as oxidant is proposed. This hybrid direct ethylene glycol fuel cell (DEGFC) is composed of a non-platinum anode, a non-platinum cathode, and a cation exchange membrane (CEM). The theoretical voltage of this hybrid DEGFC reaches 2.47 V and experimentally, the practical open-circuit voltage (OCV) is as high as 1.41V. The developed fuel cell can output a peak power density of 80.9 mW cm^{-2} at 60ºC, which is 20.8% higher than that of using oxygen (67 mW cm^{-2}) [28]. In addition, the effects of operating conditions on the cell performance were studied.

2. Working principle

As shown in Figure 1, the hybrid DEGFC consists of an anode diffusion layer (DL), an anode catalyst layer (CL), a CEM, a cathode CL, and a cathode DL. In the anode where ethylene glycol oxidation reaction (EGOR) takes place, the EG reacts with OH^- to produce oxalate, electrons, and water according to [18]:

$$C_2H_6O_2+10OH^-\rightarrow(COO^-)_2+8e^-+8H_2O \qquad E_{EGOR}=-0.69\ V \qquad (1)$$

Then the produced electrons transport from the external circuit and reach the cathode CL, participating in the hydrogen peroxide reduction reaction (HPRR), to react with hydrogen peroxide and protons to generate water according to [29]:

$$4H_2O_2+8H^++8e^-\rightarrow 8H_2O \qquad E_{HPRR}=1.78\ V \qquad (2)$$

The sodium ions transport through the CEM from the anode to the cathode to form the ionic current. Therefore, combining the Eqs. (1) and (2), the overall reaction of the hybrid DEGFC can be obtained as follows:

$$C_2H_6O_2+4H_2O_2+8H^++10OH^-\rightarrow(COO^-)_2+16H_2O \qquad E=2.47\ V \qquad (3)$$

Although the theoretical voltage of this hybrid DEGFC is so high, the practical voltage exhibits a severe degradation due to the activation loss, ohmic loss, as well as concentration loss. In addition, the mixed potential in the cathode, lowering the cell voltage, needs to be paid special attention to.

3. Experimental

3.1. Membrane electrode assembly

Three membrane electrode assemblies (MEAs) were synthesized using the identical anode electrode and cathode electrode with the same active area of 1.0 cm × 1.0 cm, as well as different CEMs with various thicknesses, *i.e.* N115 (125 μm), N117 (175 μm), and N212 (50 μm). The method for preparing the Pd/C anode was reported previously [30]. A catalyst ink was prepared by mixing 10 wt. % Pd/C (Sigma-Aldrich Co., USA) with a loading of 1.0 mg_{Pd} cm^{-2}, ethanol as the solvent and 5 wt. % Nafion as the binder. The anode catalyst ink was stirred continuously in an ultrasonic bath for 20 min, making it well dispersed. Subsequently, the anode catalyst ink was brushed onto a piece of nickel foam (Jiayisheng, China) that served as the backing layer to form an anode electrode. The preparation of cathode electrode is similar to that of anode electrode. The catalyst ink was prepared by mixing 60 wt. % Au/C (Premetek Co., USA) with a loading of

2.66 mg_{Au} cm^{-2}, ethanol as the solvent and 15 wt. % Nafion as the binder. After being ultrasonically stirred for 20 min, the catalyst ink was sprayed onto a piece of carbon cloth (Hesen, China) that served as the backing layer to form a cathode electrode. The CEMs can be obtained by treating pristine Nafion membranes as follows [30]: (1) immerse the membranes into 2.5 M NaOH solution; (2) heat up the solution to 80°C for 1 h; and (3) wash the membranes with DI water for several times. The CEMs can be stored in DI water before assembling.

3.2. Fuel cell setup and instrumentation

Each MEA was fixed between an anode plate and a cathode plate, both of which were made of 316 L stainless steel plates with flow fields. The flow field was a single serpentine flow channel grooved by the wire-cut technique, which was 0.5 mm deep and 1.0 mm wide. Two peristaltic pumps were used to feed a solution containing EG and NaOH and a solution containing H_2O_2 and H_2SO_4 to the anode and the cathode, respectively. Both of the flow rates of anode and cathode were 2.0 mL min^{-1}. Two electrical heating rods were installed to heat up the cell, and the temperature was measured by a thermocouple and controlled by a temperature controller. The polarization curves were measured by an Arbin BT2000 (Arbin Instrument Inc.) and the internal resistance was measured by the built-in function of the Arbin BT2000.

4. Results and discussion

4.1. Characterization of the cathode catalyst layer

Figure 2 shows the SEM image of the cathode CL. It can be seen that the carbon supported Au nanoparticles were uniformly distributed on the carbon cloth. Tremendous pores were formed in the CL. The porous structure provides not only large specific surface area for the electrochemical reactions, but also sufficient pathway for the mass transport. It is also shown that the distribution of Au/C nanoparticles was uniform as well, and no obvious agglomeration was observed, which is advantageous to supply numerous active sites for electrochemical reactions.

4.2. General performance

Figure 3 presents the polarization and power density curves of the hybrid DEGFC with n solution containing 1.0 M EG and 7.0 M NaOH at a flow rate of 2.0 mL min^{-1} fed into anode as well as a solution containing 1.0 M H_2SO_4 and 4.0 M H_2O_2 at a flow rate of 2.0 mL min^{-1} fed into cathode at 80ºC. It demonstrates that a peak power density of 115.3 mW cm^{-2} and an OCV of 1.43 V were achieved. The performance shows significant improvements both in peak power density and OCV when comparing with the results of previous work (67 mW cm^{-2} and 0.86 V at 60ºC) [28]. The main reason accounting for the phenomenon is that the HPRR igoes through a two-electron transfer process, which is more favorable due to the faster electrochemical kinetics comparing with the four-electron-transfer ORR process [31]. In spite of the performance improvement, the actual voltage (1.41 V) is much less than the theoretical voltage (2.47 V). The reason why the practical voltage is relatively low is explained as follows. As H_2O_2 is not stable and is more likely to be oxidized to produce oxygen, protons, and electrons at a high potential [32], this oxidation reaction together with HPRR can spontaneously establish a hydrogen peroxide-based fuel cells at the cathode.

$$H_2O_2 \rightarrow O_2 + 2H^+ + 2e^- \qquad E_{HPOR}=0.69\ V \qquad (4)$$

Hence, the cathode potential decreases as a result of the mixed potential. Additionally, the produced oxygen is probable to be reduced in the cathode according to:

$$O_2 + 4H^+ + 4e^- \rightarrow 2H_2O \qquad E_{ORR}=1.23\ V \qquad (5)$$

The ORR potential is not as high as the HPRR potential, which is another possible reason for the unexpected voltage. The constant-current discharging behavior of this hybrid DEGFC is presented in Figure 4. The constant current was set to be 50 mA cm^{-2}. It can be seen that the fuel

cell exhibits a rather stable performance in 4-hour continuous operation, indicating that this DEGFC possesses the potential for future applications.

4.3. Effect of NaOH concentration

Figure 5 (a) shows the effect of the NaOH concentration on the cell performance with EG concentration fixed at 1.0 M. It is shown that the cell voltage increased with the NaOH concentration initially, and decreased subsequently over the whole current density range. And the OCV increased when the OH^- concentration increased from 1.0 M to 7.0 M. This phenomenon can be explained that for a specific electrocatalyst, the kinetics of EGOR primarily depends on the local concentration of EG and OH^- in the anode CL. As the concentration of EG is fixed at 1.0 M, the increase in OH^- concentration leads to the OH^- concentration in the anode CL transferring from starving state to sufficient state, which is beneficial for enhancing the EGOR kinetics. However, further increasing the OH^- concentration from 7.0 M to 9.0 M did not contribute to higher OCV. The reason for this behavior is that high OH^- concentration leads to more active sites being covered by OH^-, which may hinder the EG adsorption on the active sites. The adsorption competition between EG and OH^- may cause the EG concentration in a starving state [33], resulting in the voltage degradation as shown in Figure 5 (b). It is seen that the highest peak power density of 80.9 mW cm^{-2} was achieved at 7.0 M, while either higher or lower OH^- concentration would result in the performance decline. In general, the alkalinity of the anode not only affects the electrochemical kinetics, but also influences the transport of species in the anode, including EG, OH^-, and Na^+. Figure 5 (b) shows that the internal resistance increased from 408 mOhm to 931 mOhm with the NaOH concentration increasing from 1.0 M to 9.0 M, suggesting that the mass/charge transport is impeded and the ohmic loss is enhanced. On one hand, although the ohmic loss increases with increasing the OH^- concentration, resulting in the performance

degradation, the performance promotion that is attributed to the facilitated EGOR kinetics can compensate the negative performance decline to achieve the positive overall effect from 1.0 M to 7.0 M. Therefore, the overall performance increases with the NaOH concentration increasing from 1.0 M to 7.0 M. On the other hand, too high OH^- concentration will occupy the active sites and suppress the EG adsorption, leading to higher concentration loss. The combination of the reduced EGOR kinetics and undesirable ohmic loss causes the inferior performance at 9.0 M.

4.4. Effect of EG concentration

The effect of EG concentration on the cell performance was also studied when the NaOH concentration was fixed at 7.0 M, as shown in Figure 6 (a). It is seen that the cell voltage increased with the EG concentration initially, and decreased subsequently over the whole current density range. The reasons for this behavior can be explained as follows. As the EG concentration increases from 0.5 M to 1.0 M, the transport of EG to active sites is accelerated, lowering the concentration loss and improving the OCV, as shown in Figure 6 (b). This is evidenced by the fact that the performance experienced a severe degradation from 150 mA cm^{-2} to 160 mA cm^{-2}, which is attributed to significant concentration loss due to the lack of EG in the anode CL. In contrast, no obvious concentration loss was observed in high current density region under 1.0 M operation. As the EG concentration further increased from 1.0 M to 2.0 M, the cell voltage exhibited a small degradation. One reason for the decline is the presence of adsorption competition between EG and OH^-. A higher EG concentration may arrogate the active sites, preventing the OH^- from participating in the EGOR. In addition, the EG crossover from the anode to the cathode is enhanced with the increased EG concentration. As the mixed potential increases resulting from more EG reaching the cathode, the cathode potential will degrade, leading to a lower OCV. As a result, the OCV decreases derived from the increased

concentration loss of OH^- and the subdued electrochemical kinetics. The other is that the increasing viscosity of anolyte due to the higher EG concentration restricts the mass/charge transport in the anode, which is verified by Figure 6 (b). The internal resistance increases with the EG concentration, thus the ohmic loss boosts simultaneously, declining the cell performance.

4.5. Effect of H_2O_2 concentration

Figure 7 (a) shows the effect of hydrogen peroxide concentration on the cell performance when the sulfuric acid concentration was fixed at 1.0 M. It is seen that the cell voltage first decreased in the low current density region and then increased, finally followed by a voltage drop when the hydrogen peroxide concentration increased from 1.0 M to 6.0 M as depicted in Figure 7 (b). The cell voltage first increased and then decreased with increasing hydrogen peroxide concentration in the high current density region. At the low current density region, the decreased voltage with the H_2O_2 concentration increasing from 1.0 M to 2.0 M is mainly ascribed to the H_2O_2 crossover from the cathode to the anode [34]. The permeated H_2O_2 will react with EG in the anode and produce a mixed potential, lowering the anode potential and thus the overall voltage. Afterwards, the voltage increased with the H_2O_2 concentration increasing from 2.0 M to 4.0 M. The reason for this phenomenon is that although the crossover becomes more serious with higher H_2O_2 concentration, the higher H_2O_2 concentration also transfers the starving state to sufficient state in the cathode CL, enhancing the HPRR kinetics. As a consequence, the positive effect on the cell voltage exceeds the negative effect, exhibiting an improved performance. However, further increasing the H_2O_2 concentration did not present a continuous enhancement. It can be explained that the H_2O_2 in the CL is sufficient at 4.0 M, so further increasing the H_2O_2 concentration to 6.0 M brings out the adsorption competition between H_2O_2 and H^+. Therefore, the concentration loss of H^+ is elevated. Meanwhile, accompanying with the negative effect derived from the severer

H_2O_2 crossover, the cell voltage showed a degradation when the H_2O_2 concentration increases from 4.0 M to 6.0 M. At a high current density region, the reason for the voltage increasing with the H_2O_2 concentration from 1.0 M to 4.0 M is attributed to the sufficient supply of H_2O_2 in the cathode CL, reducing the cathode concentration loss of H_2O_2 and thus promoting the cell voltage. While the H_2O_2 concentration increased to 6.0 M, the performance degraded. because the reason is that the internal resistance increases with H_2O_2 concentration, which is evidenced by the Figure 7 (b). A higher internal resistance results in a high ohmic loss, leading to the voltage degradation. Moreover, the mixed potential in the anode is enhanced due to the severer H_2O_2 crossover, elevating the anode potential and thus lowering the overall cell voltage.

4.6. Effect of H_2SO_4 concentration

The effect of sulfuric acid concentration on the cell performance was investigated with the hydrogen peroxide concentration fixed at 4.0 M, and the results were shown in Figure 8 (a). It is seen that the cell voltage increased with the H_2SO_4 concentration initially, and decreased subsequently over the whole current density range. The explanation for the increased voltage from 0.5 M to 1.0 M is that the transport of H^+ to active sites is enhanced, which reduces the concentration loss of H^+ and promotes the cell voltage as shown in Figure 8 (b) [35]. However, a higher H_2SO_4 concentration exceeding 1.0 M did not contribute to a higher cell performance. This behavior is mainly attributed to two reasons. One is that numerous active sites are covered by the redundant H_2SO_4, resulting in the shortage of H^+ in the CL and higher concentration loss of H^+, so that the cell voltage degrades. The other is that the viscosity of catholyte increases with the H_2SO_4 concentration, leading to the linear rise in the internal resistance as depicted in Figure 8 (b), which causes the enhanced ohmic loss. Therefore, the cell performance underwent a significant degradation at 2.0 M due to the synergetic negative effect.

4.7. Effect of membrane thickness

The effect of membrane thickness on the cell performance was studied and the results were shown in Figure 9 (a). It is seen that the cell with a thinner membrane yielded a superior performance over almost the whole current density range, whereas the cell with a thicker membrane exhibited a superior OCV. As shown in Figure 9 (b), both of the OCV and internal resistance were increasing with the membrane thickness. Since the membrane becomes thicker, the EG crossover from the anode to cathode is suppressed. As a result, the EG crossover form the anode to the cathode is hindered, lowering the mixed potential in the cathode so that both the cathode potential and the OCV increases. However, when the cell was discharging, the ohmic loss needed to be taken into consideration. Over the whole current density range, the cell with a thicker membrane experienced a rapider voltage degradation due to the higher ohmic loss. It is indicated that the positive effect derived from the reduced mixed potential in the cathode is too deficient to compensate the negative effect owing to the substantial internal resistance, suggesting that the internal resistance plays the predominant role in the cell performance.

4.8. Effect of temperature

Figure 10 shows the effect of operating temperature on the cell performance. It is seen that the cell performance increased with the operating temperature. The peak power densities were 49.3, 80.9, and 115.3 mW cm^{-2} when the cell was operated at 40ºC, 60ºC, and 80ºC, respectively. The reasons for this remarkable improvement with the operating temperature can be concluded as follows. On one hand, both the kinetics of the EGOR in the anode and the HPRR in the cathode will be facilitated at higher operating temperatures, resulting in the decreased activation loss [36]. On the other hand, increasing operating temperature is beneficial for accelerating the reactants transport in both of the anode and the cathode as well as the ion transport through the membrane. As the reactants deliver to the active sites more easily, the concentration loss of both anode and

cathode due to the reactant shortage is reduced. In addition, the conductivity of the membrane increases and thus the internal resistance decreases, which lowers the ohmic loss. Therefore, the cell performance upgrades with operating temperature.

5. Conclusion

In this work, a hybrid direct ethylene glycol fuel cell has been developed and tested. The effects of operation conditions on the cell performance have been also examined. It is demonstrated that the peak power densities were 80.9 mW cm^{-2} and 115.3 mW cm^{-2} with an aqueous solution containing 1.0 M EG and 7.0 M NaOH at a flow rate of 2.0 mL min^{-1} fed into anode as well as an aqueous solution containing 1.0 M H_2SO_4 and 4.0 M H_2O_2 at a flow rate of 2.0 mL min^{-1} fed into cathode at 60ºC and 80ºC, respectively. The hybrid DEGFC exhibits a 20.8% increase in the peak power density at 60ºC than that in a DEGFC with oxygen as oxidant (67 mW cm^{-2}), which is ascribed to the faster kinetics of two-electron-transfer HPRR and the reduced ohmic loss. It is also shown that the operation conditions, including species concentrations both in anode and cathode, the thickness of membrane, and the operating temperature, possessed significant effects on the cell performance.

Acknowledgements:

This work was fully supported by a grant from the Research Grants Council of the Hong Kong Special Administrative Region, China (Project No. 25211817).

References

[1] Z.F. Pan, L. An, T.S. Zhao, Z.K. Tang, Advances and challenges in alkaline anion exchange membrane fuel cells, Progress in Energy and Combustion Science 66 (2018) 141-175.

[2] L. An, T.S. Zhao, Anion exchange membrane fuel cells: Principles, Materials and Systems, Springer International Publishing, Cham, Switzerland, 2018.

[3] Q.X. Wu, Z.F. Pan, L. An, Recent advances in alkali-doped polybenzimidazole membranes for fuel cell applications, Renew. Sustain. Energy Rev. 89 (2018) 168-183.

[4] C.Y. Wen, G.W. Huang, Application of a thermally conductive pyrolytic graphite sheet to thermal management of a PEM fuel cell, J. Power Sources 178 (2008) 132-140.

[5] C.Y. Wen, Y.S. Lin, C.H. Lu, Experimental study of clamping effects on the performances of a single proton exchange membrane fuel cell and a 10-cell stack, J. Power Sources 192 (2009) 475-485.

[6] L. An, R. Chen, Direct formate fuel cells: A review, J. Power Sources 320 (2016) 127-139.

[7] Y.S. Li, Y. Feng, X.D. Sun, Y.L. He, A sodium-ion-conducting direct formate fuel cell: generating electricity and producing base, Angew. Chem. 129 (2017) 5828-5831.

[8] Y.S. Li, X.D. Sun, Y. Feng, Hydroxide self-feeding high-temperature alkaline direct formate fuel cells, ChemSusChem 10 (2017) 2135-2139.

[9] C.Y. Wen, Y.S. Lin, C.H. Lu, Performance of a proton exchange membrane fuel cell stack with thermally conductive pyrolytic graphite sheets for thermal management, J. Power Sources 189 (2009) 1100-1105.

[10] T.S. Zhao, C. Xu, R. Chen, W.W. Yang, Mass transport phenomena in direct methanol fuel cells, Progress in Energy and Combustion Science 35 (2009) 275-292.

[11] L. An, T.S. Zhao, Transport phenomena in alkaline direct ethanol fuel cells for sustainable energy production, J. Power Sources 341 (2017) 199-211.

[12] L. An, T.S. Zhao, Y.S. Li, Carbon-neutral sustainable energy technology: Direct ethanol fuel cells, Renew. Sustain. Energy Rev. 50 (2015) 1462-1468.

[13] L. An, R. Chen, Mathematical modeling of direct formate fuel cells, Applied Thermal Engineering 124 (2017) 232-240.

[14] Y.S. Li, T.S. Zhao, A passive anion-exchange membrane direct ethanol fuel cell stack and its applications, Int. J. Hydrogen Energy 41 (2016) 20336-20342.

[15] Y.S. Li, Y.L. He, W.W. Yang, A high-performance direct formate-peroxide fuel cell with palladium-gold alloy coated foam electrodes, J. Power Sources 278 (2015) 569-573.

[16] Z.F. Pan, R. Chen, L. An, Y.S. Li, Alkaline anion exchange membrane fuel cells for cogeneration of electricity and valuable chemicals, J. Power Sources 365 (2017) 430-445.

[17] X.Y. Chen, T.C. Li, J.N. Shen, Z.L. Hu, From structures, packaging to application: A system-level review for micro direct methanol fuel cell, Renew. Sustain. Energy Rev. 80 (2017) 669-678

[18] L. An, R. Chen, Recent progress in alkaline direct ethylene glycol fuel cells for sustainable energy production, J. Power Sources 329 (2016) 484-501.

[19] H.R. Yue, Y.J. Zhao, X.B. Ma, J.L. Gong, Ethylene glycol: properties, synthesis, and applications, Chem. Soc. Rev. 41 (2012) 4218-4244.

[20] L. An, L. Zeng, T.S. Zhao, An alkaline direct ethylene glycol fuel cell with an alkali-doped polybenzimidazole membrane, Int. J. Hydrogen Energy 38 (2013) 10602-10606.

[21] C.Y. Wen, Y.S. Lin, C.H. Lu, T.W. Luo, Thermal management of a proton exchange membrane fuel cell stack with pyrolytic graphite sheets and fans combined, Int. J. Hydrogen Energy 36 (2011) 6082-6089.

[22] L. An, T.S. Zhao, X.H. Yan, X.L. Zhou, P. Tan, The dual role of hydrogen peroxide in fuel cells, Science Bulletin 60 (2015) 55-64.

[23] E.H. Yu, U. Krewer, K. Scott, Principles and materials aspects of direct alkaline alcohol fuel cells, Energies 3 (2010) 1499-1528.

[24] G.F. McLean, T. Niet, S. Prince-Richard, N. Djilali, An assessment of alkaline fuel cell technology, Int. J. Hydrogen Energy 27 (2002) 507-526.

[25] L. An, T.S. Zhao, Z.H. Chai, L. Zeng, P. Tan, Modeling of the mixed potential in hydrogen peroxide-based fuel cells, Int. J. Hydrogen Energy 39 (2014) 7407-7416.

[26] L. An, C.Y. Jung, Transport phenomena in direct borohydride fuel cells, Applied Energy 205 (2017) 1270-1282.

[27] S. Fukuzumi, Y. Yamada, Hydrogen peroxide used as a solar fuel in one-compartment fuel cells, ChemElectroChem 3 (2016) 1978-1989.

[28] L. An, T.S. Zhao, S.Y. Shen, Q.X. Wu, R. Chen, Performance of a direct ethylene glycol fuel cell with an anion-exchange membrane, Int. J. Hydrogen Energy 35 (2010) 4329-4335.

[29] L. An, T.S. Zhao, R. Chen, Q.X. Wu, A novel direct ethanol fuel cell with high power density, J. Power Sources 196 (2011) 6219-6222.

[30] L. An, T.S. Zhao, Performance of an alkaline-acid direct ethanol fuel cell, Int. J. Hydrogen Energy 36 (2011) 9994-9999.

[31] G.H. Miley, N. Luo, J. Mather, R. Burton, G. Hawkins, L.F. Gu, E. Byrd, R. Gimlin, P.J. Shrestha, G. Benavides, J. Laystrom, D. Carroll, Direct $NaBH_4/H_2O_2$ fuel cells, J. Power Sources 165 (2007) 509-516.

[32] X. Jing, D.X. Cao, Y. Liu, G.L. Wang, J.L. Yin, Q. Wen, Y.Y. Gao, The open circuit potential of hydrogen peroxide at noble and glassy carbon electrodes in acidic and basic electrolytes, J. Electroanalytical Chemistry 658 (2011) 46-51.

[33] Y.S. Li, T.S. Zhao, Z.X. Liang, Performance of alkaline electrolyte-membrane based direct ethanol fuel cells, J. Power Sources 187 (2009) 387-392.

[34] Integrated electrochemical/chemical oxygen generating system. US 4,488,951; Dec. 18, 1984.

[35] R.K. Raman, N.A Choudhury, A.K. Shukla, A high output voltage direct borohydride fuel cell, Electrochem Solid-State Lett. 7 (2004) A488-491.

[36] Y.S. Li, T.S. Zhao, A high-performance integrated electrode for anion-exchange membrane direct ethanol fuel cells, Int. J. Hydrogen Energy 36 (2011) 7707-7713.

Figure captions:

Figure 1 Schematic of the hybrid DEGFC.

Figure 2 SEM image of the cathode catalyst layer.

Figure 3 Polarizaiton and power density curves of the hybrid DEGFC. Anode: 1.0 M EG and 7.0 M NaOH aqueous solution, 2.0 mL min^{-1}. Cathode: 1.0 M H_2SO_4 and 4.0 M H_2O_2 aqueous solution, 2.0 mL min^{-1}. Membrane: Nafion 212. Temperature: 80ºC.

Figure 4 Constant-current discharging behavior. Anode: 1.0 M EG and 7.0 M NaOH aqueous solution, 2.0 mL min^{-1}. Cathode: 1.0 M H_2SO_4 and 4.0 M H_2O_2 aqueous solution, 2.0 mL min^{-1}. Membrane: Nafion 212. Temperature: 60ºC.

Figure 5 (a) Effect of the NaOH concentration on the cell performance. Anode: 1.0 M EG and various NaOH concentration aqueous solution, 2.0 mL min^{-1}. Cathode: 1.0 M H_2SO_4 and 4.0 M H_2O_2 aqueous solution, 2.0 mL min^{-1}. Membrane: Nafion 212. Temperature: 60ºC.

Figure 5 (b) Effect of the NaOH concentration on the internal resistance. Anode: 1.0 M EG and various NaOH concentration aqueous solution, 2.0 mL min^{-1}. Cathode: 1.0 M H_2SO_4 and 4.0 M H_2O_2 aqueous solution, 2.0 mL min^{-1}. Membrane: Nafion 212. Temperature: 60ºC.

Figure 6 (a) Effect of the EG concentration on the cell performance. Anode: various EG concentration and 7.0 M NaOH aqueous solution, 2.0 mL min^{-1}. Cathode: 1.0 M H_2SO_4 and 4.0 M H_2O_2 aqueous solution, 2.0 mL min^{-1}. Membrane: Nafion 212. Temperature: 60ºC.

Figure 6 (b) Effect of the EG concentration on the internal resistance. Anode: various EG concentration and 7.0 M NaOH aqueous solution, 2.0 mL min^{-1}. Cathode: 1.0 M H_2SO_4 and 4.0 M H_2O_2 aqueous solution, 2.0 mL min^{-1}. Membrane: Nafion 212. Temperature: 60ºC.

Figure 7 (a) Effect of the H_2O_2 concentration on the cell performance. Anode: 1.0 M EG and 7.0 M NaOH aqueous solution, 2.0 mL min^{-1}. Cathode: 1.0 M H_2SO_4 and various H_2O_2 concentration aqueous solution, 2.0 mL min^{-1}. Membrane: Nafion 212. Temperature: 60ºC.

Figure 7 (b) Effect of the H_2O_2 concentration on the internal resistance. Anode: 1.0 M EG and 7.0 M NaOH aqueous solution, 2.0 mL min^{-1}. Cathode: 1.0 M H_2SO_4 and various H_2O_2 concentration aqueous solution, 2.0 mL min^{-1}. Membrane: Nafion 212. Temperature: 60ºC.

Figure 8 (a) Effect of the H_2SO_4 concentration on the cell performance. Anode: 1.0 M EG and 7.0 M NaOH aqueous solution, 2.0 mL min^{-1}. Cathode: various H_2SO_4 concentration and 4.0 M H_2O_2 aqueous solution, 2.0 mL min^{-1}. Membrane: Nafion 212. Temperature: 60ºC.

Figure 8 (b) Effect of the H_2SO_4 concentration on the internal resistance. Anode: 1.0 M EG and 7.0 M NaOH aqueous solution, 2.0 mL min^{-1}. Cathode: various H_2SO_4 concentration and 4.0 M H_2O_2 aqueous solution, 2.0 mL min^{-1}. Membrane: Nafion 212. Temperature: 60ºC.

Figure 9 (a) Effect of the membrane thickness on the cell performance. Anode: 1.0 M EG and 7.0 M NaOH aqueous solution, 2.0 mL min^{-1}. Cathode: 1.0 M H_2SO_4 and 4.0 M H_2O_2 aqueous solution, 2.0 mL min^{-1}. Temperature: 60ºC.

Figure 9 (b) Effect of the membrane thickness on the internal resistance. Anode: 1.0 M EG and 7.0 M NaOH aqueous solution, 2.0 mL min^{-1}. Cathode: 1.0 M H_2SO_4 and 4.0 M H_2O_2 aqueous solution, 2.0 mL min^{-1}. Temperature: 60ºC.

Figure 10 Effect of the temperature on the cell performance. Anode: 1.0 M EG and 7.0 M NaOH aqueous solution, 2.0 mL min^{-1}. Cathode: 1.0 M H_2SO_4 and 4.0 M H_2O_2 aqueous solution, 2.0 mL min^{-1}. Membrane: Nafion 212.

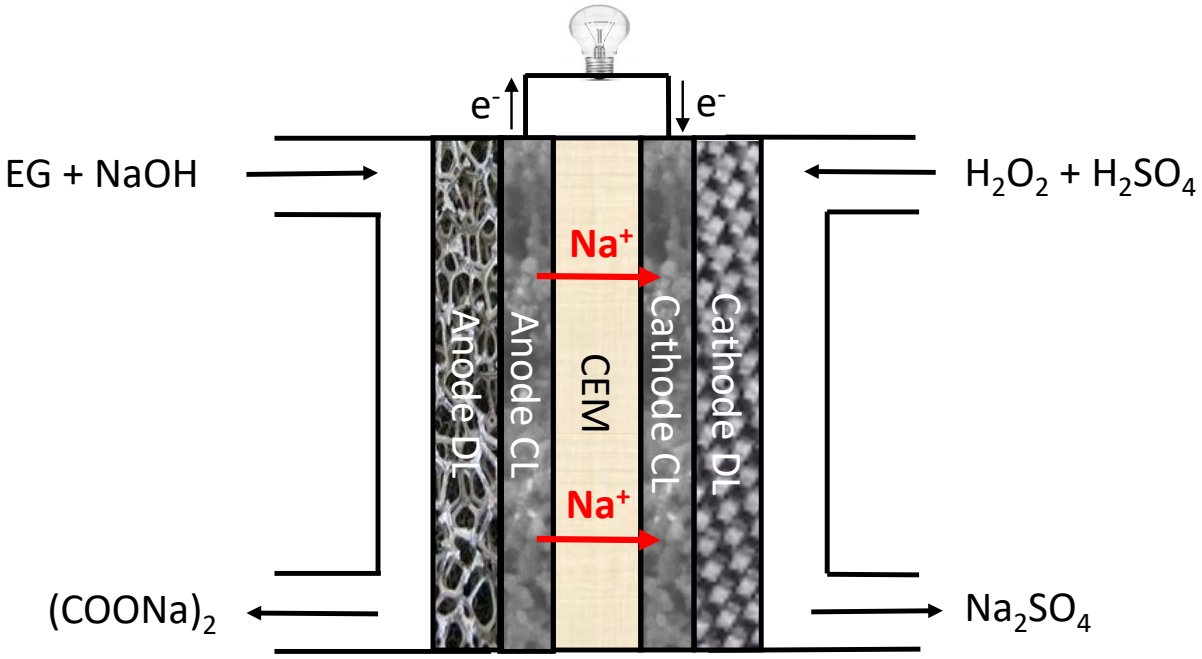

Figure 1 Schematic of the hybrid DEGFC.

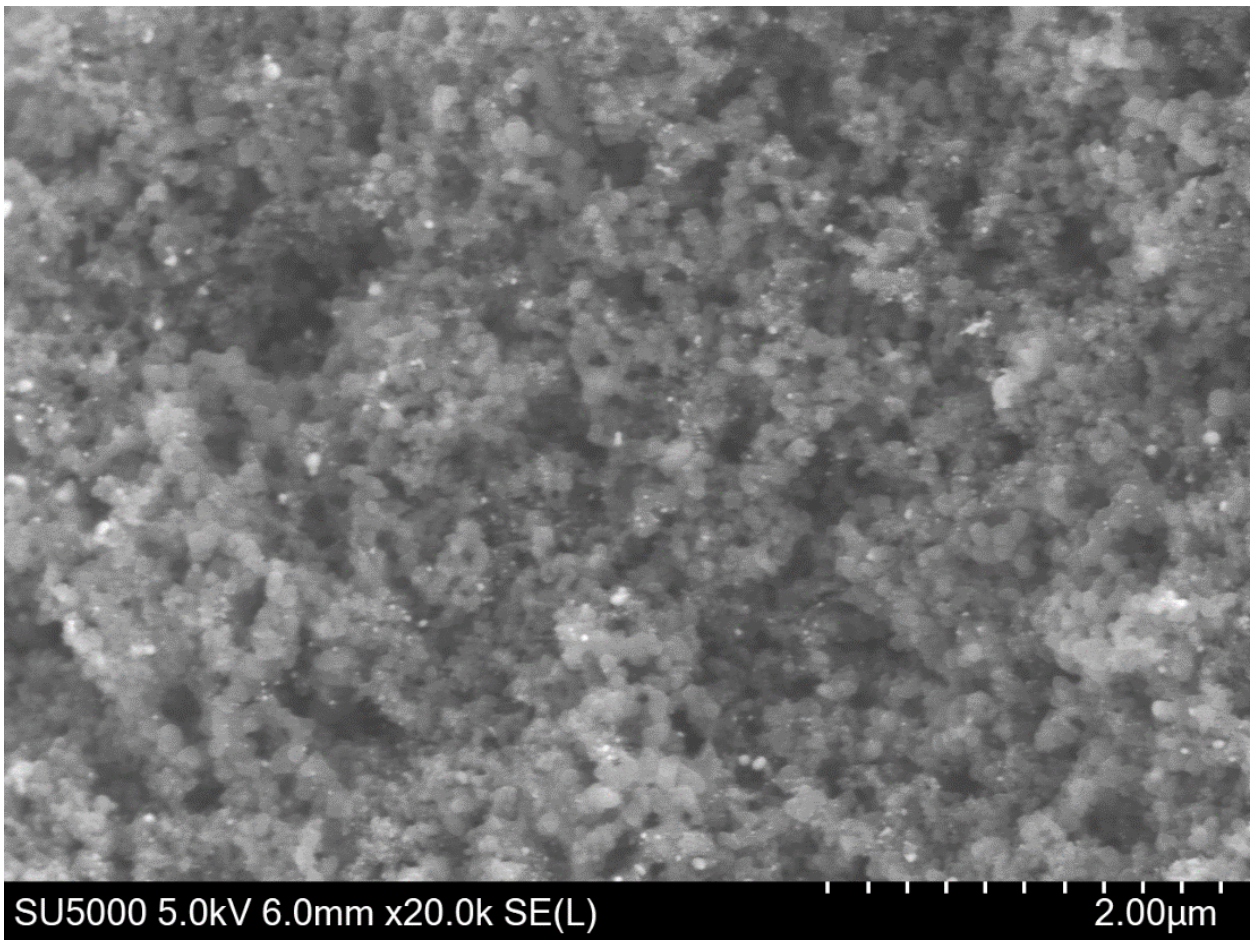

Figure 2 SEM image of the cathode catalyst layer.

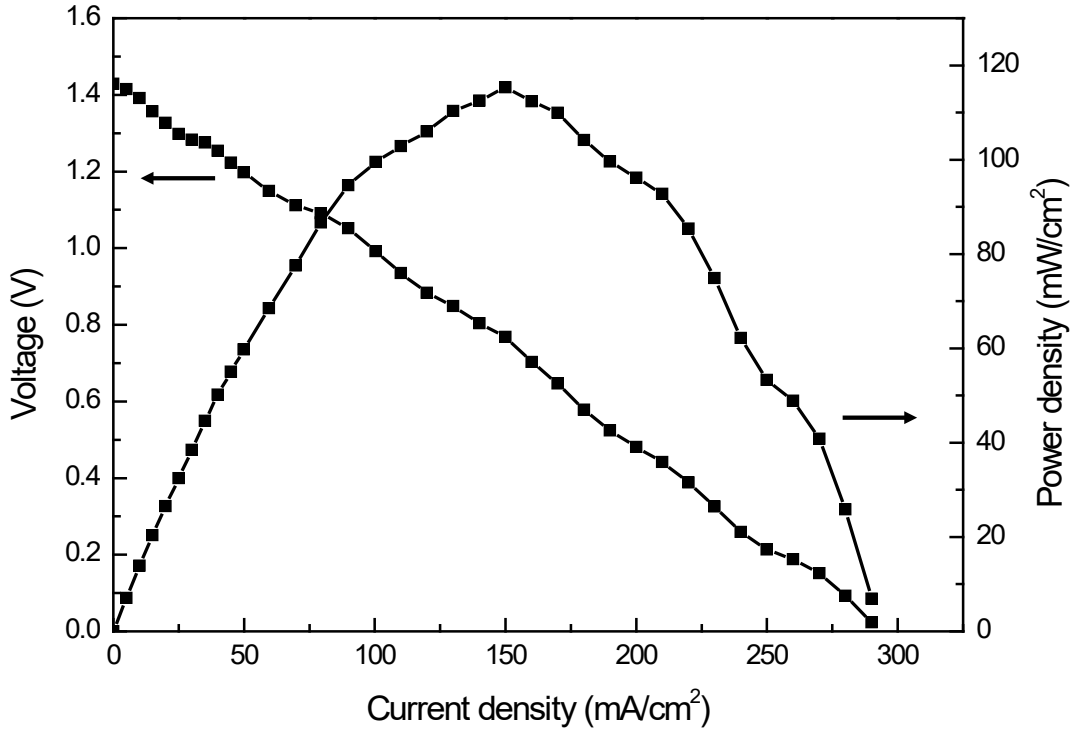

Figure 3 Polarizaiton and power density curves of the hybrid DEGFC. Anode: 1.0 M EG and 7.0 M NaOH aqueous solution, 2.0 mL min^{-1}. Cathode: 1.0 M H_2SO_4 and 4.0 M H_2O_2 aqueous solution, 2.0 mL min^{-1}. Membrane: Nafion 212. Temperature: 80^{o}C.

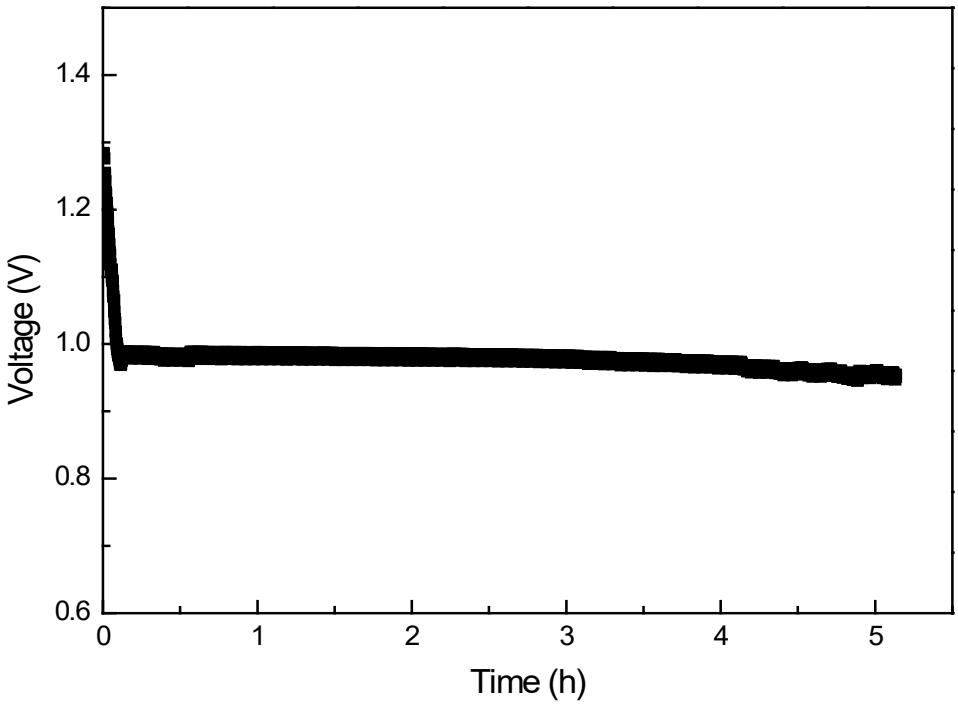

Figure 4 Constant-current discharging behavior. Anode: 1.0 M EG and 7.0 M NaOH aqueous solution, 2.0 mL min^{-1}. Cathode: 1.0 M H_2SO_4 and 4.0 M H_2O_2 aqueous solution, 2.0 mL min^{-1}. Membrane: Nafion 212. Temperature: 60°C.

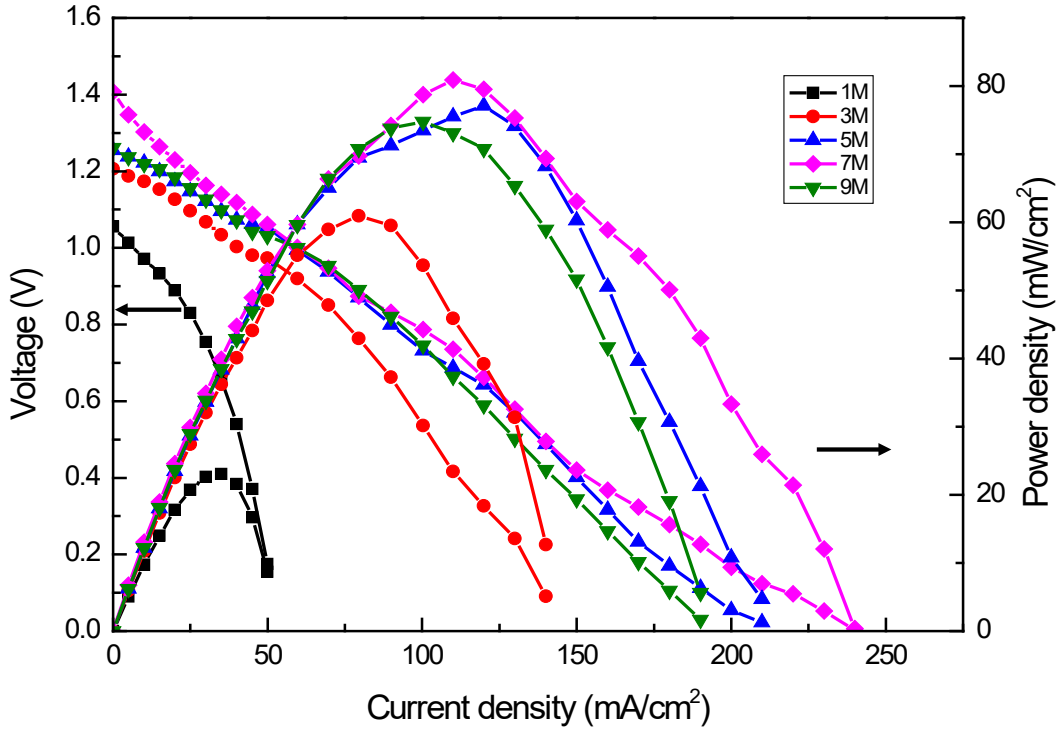

Figure 5 (a) Effect of the NaOH concentration on the cell performance. Anode: 1.0 M EG and various NaOH concentration aqueous solution, 2.0 mL min^{-1}. Cathode: 1.0 M H_2SO_4 and 4.0 M H_2O_2 aqueous solution, 2.0 mL min^{-1}. Membrane: Nafion 212. Temperature: 60°C.

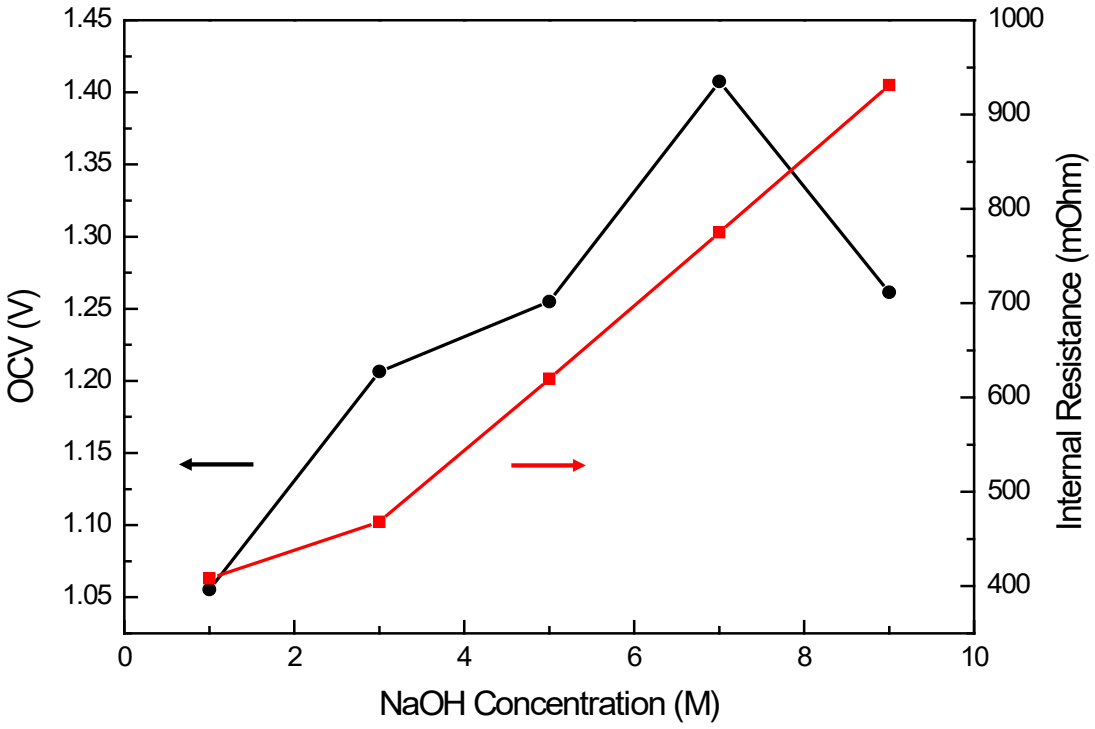

Figure 5 (b) Effect of the NaOH concentration on the internal resistance. Anode: 1.0 M EG and various NaOH concentration aqueous solution, 2.0 mL min^{-1}. Cathode: 1.0 M H_2SO_4 and 4.0 M H_2O_2 aqueous solution, 2.0 mL min^{-1}. Membrane: Nafion 212. Temperature: 60°C.

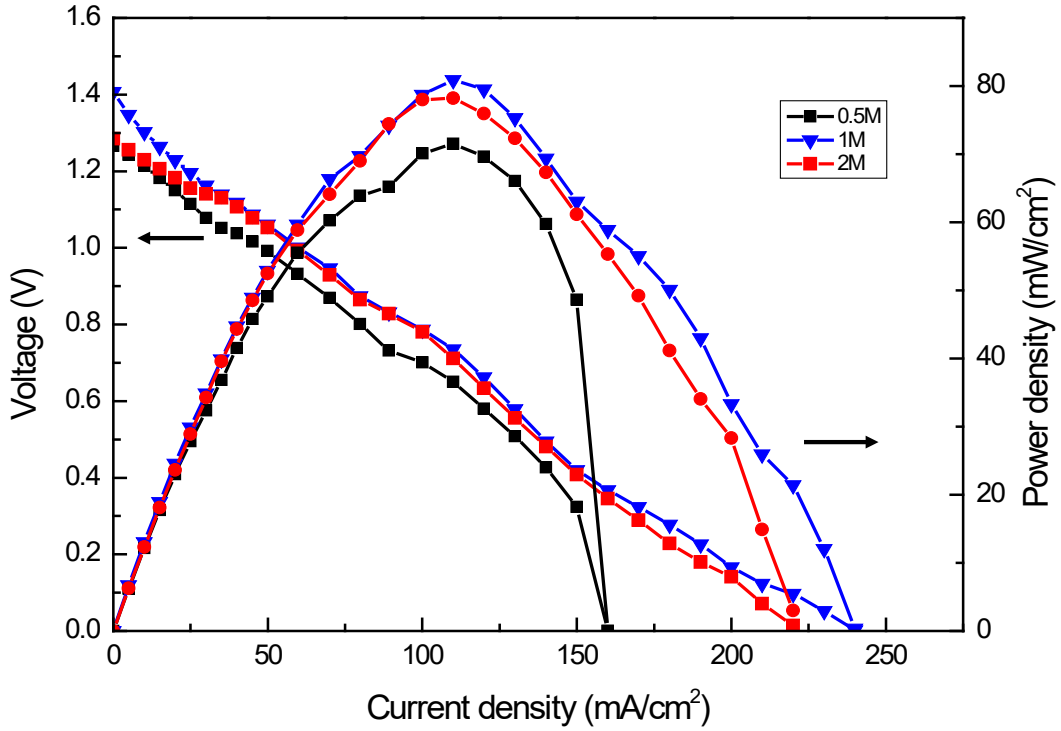

Figure 6 (a) Effect of the EG concentration on the cell performance. Anode: various EG concentration and 7.0 M NaOH aqueous solution, 2.0 mL min^{-1}. Cathode: 1.0 M H_2SO_4 and 4.0 M H_2O_2 aqueous solution, 2.0 mL min^{-1}. Membrane: Nafion 212. Temperature: 60^{o}C.

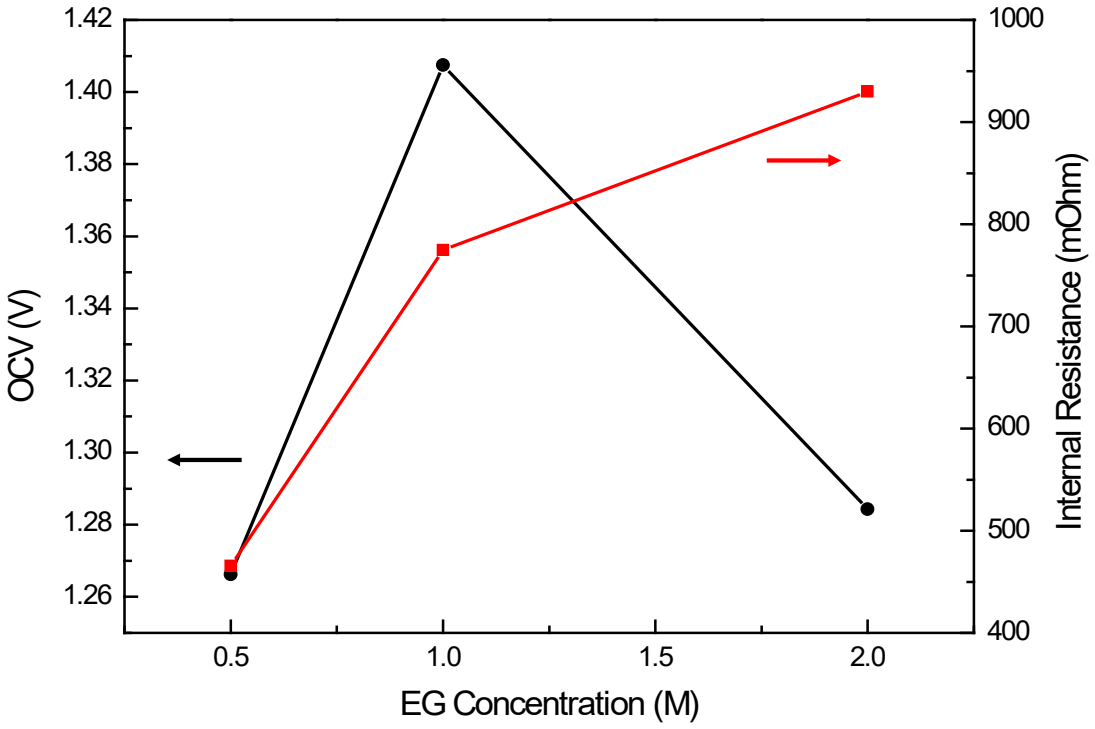

Figure 6 (b) Effect of the EG concentration on the internal resistance. Anode: various EG concentration and 7.0 M NaOH aqueous solution, 2.0 mL min^{-1}. Cathode: 1.0 M H_2SO_4 and 4.0 M H_2O_2 aqueous solution, 2.0 mL min^{-1}. Membrane: Nafion 212. Temperature: 60°C.

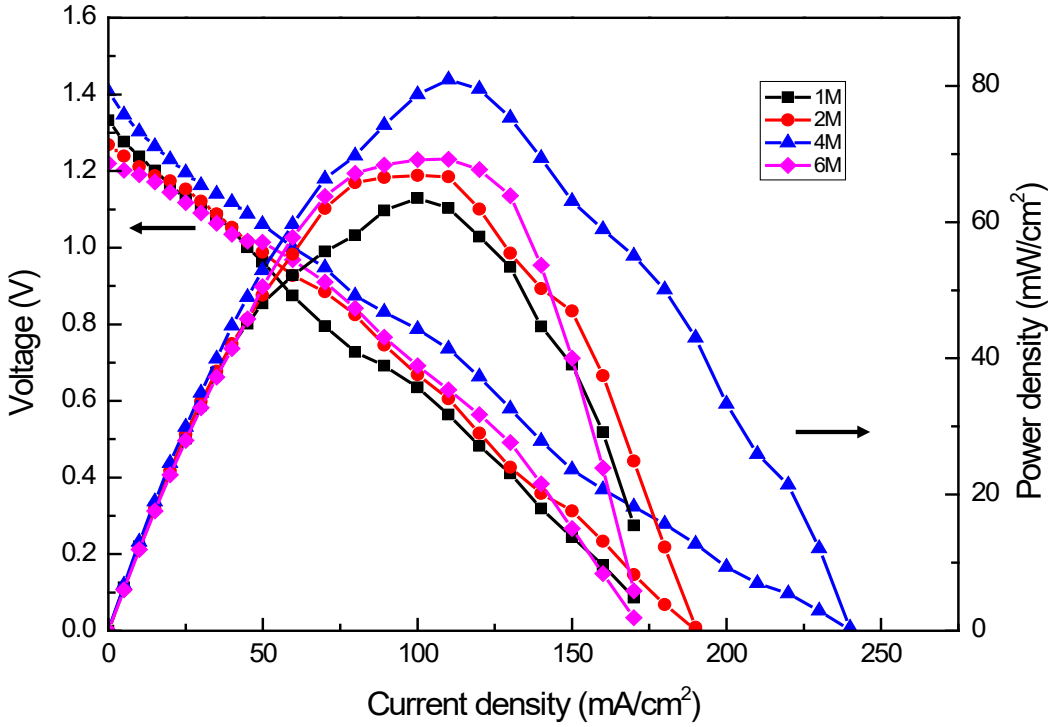

Figure 7 (a) Effect of the H_2O_2 concentration on the cell performance. Anode: 1.0 M EG and 7.0 M NaOH aqueous solution, 2.0 mL min^{-1}. Cathode: 1.0 M H_2SO_4 and various H_2O_2 concentration aqueous solution, 2.0 mL min^{-1}. Membrane: Nafion 212. Temperature: 60ºC.

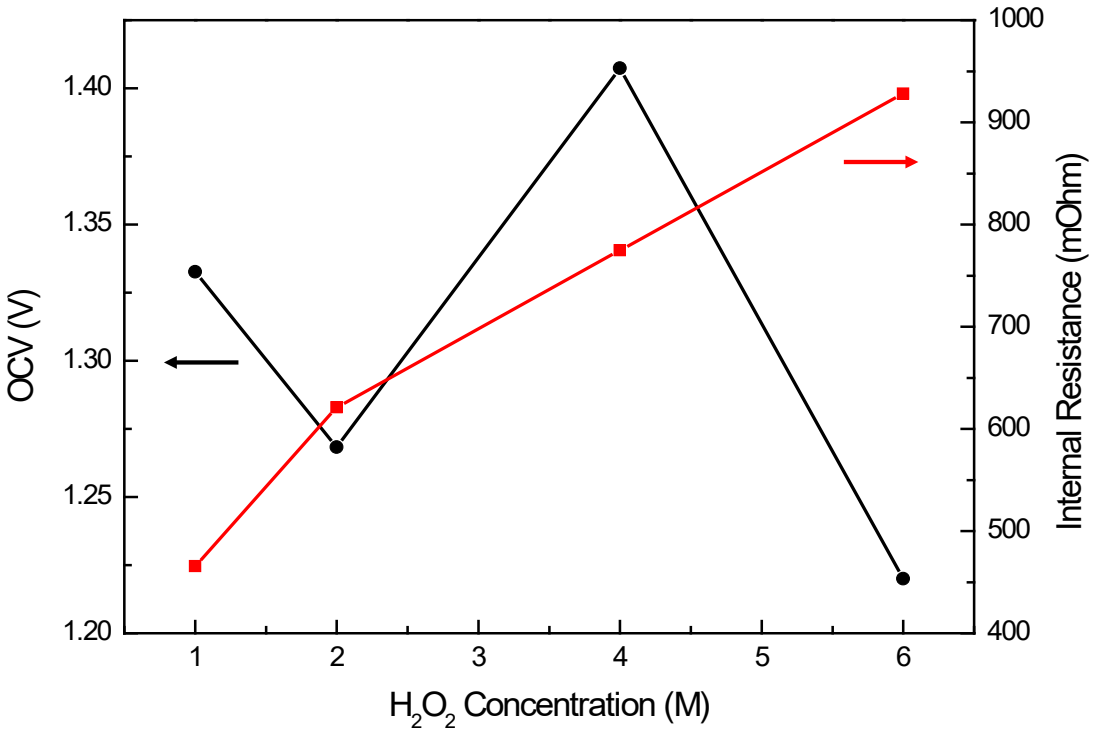

Figure 7 (b) Effect of the H_2O_2 concentration on the internal resistance. Anode: 1.0 M EG and 7.0 M NaOH aqueous solution, 2.0 mL min^{-1}. Cathode: 1.0 M H_2SO_4 and various H_2O_2 concentration aqueous solution, 2.0 mL min^{-1}. Membrane: Nafion 212. Temperature: 60°C.

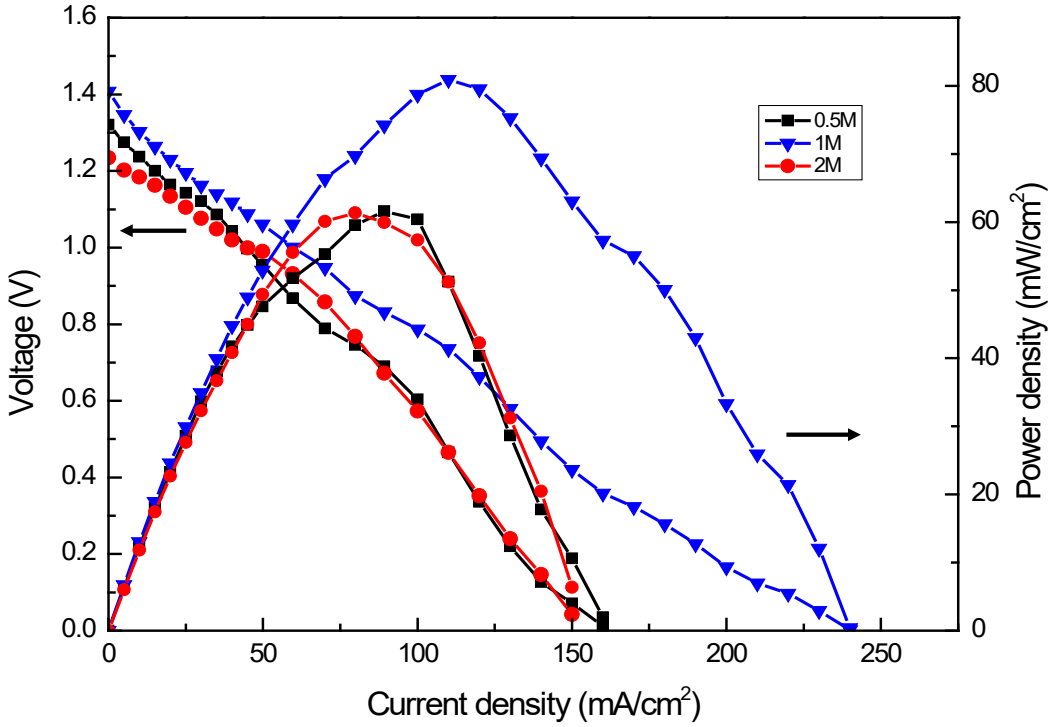

Figure 8 (a) Effect of the H_2SO_4 concentration on the cell performance. Anode: 1.0 M EG and 7.0 M NaOH aqueous solution, 2.0 mL min^{-1}. Cathode: various H_2SO_4 concentration and 4.0 M H_2O_2 aqueous solution, 2.0 mL min^{-1}. Membrane: Nafion 212. Temperature: 60ºC.

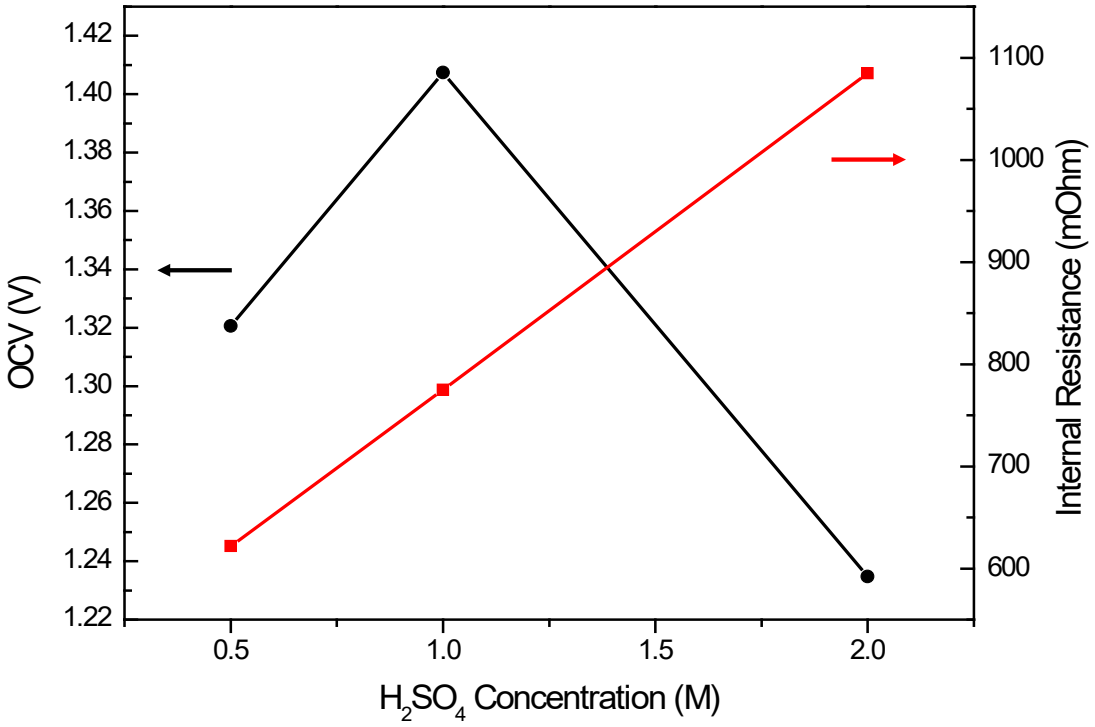

Figure 8 (b) Effect of the H_2SO_4 concentration on the internal resistance. Anode: 1.0 M EG and 7.0 M NaOH aqueous solution, 2.0 mL min^{-1}. Cathode: various H_2SO_4 concentration and 4.0 M H_2O_2 aqueous solution, 2.0 mL min^{-1}. Membrane: Nafion 212. Temperature: 60°C.

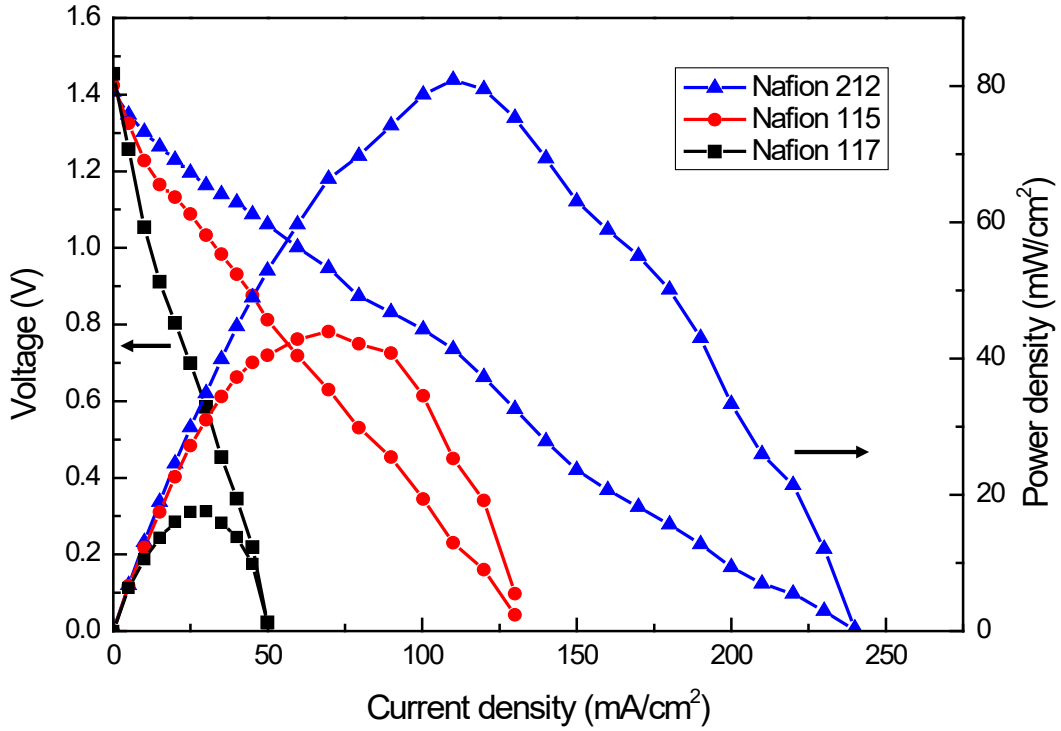

Figure 9 (a) Effect of the membrane thickness on the cell performance. Anode: 1.0 M EG and 7.0 M NaOH aqueous solution, 2.0 mL min^{-1}. Cathode: 1.0 M H_2SO_4 and 4.0 M H_2O_2 aqueous solution, 2.0 mL min^{-1}. Temperature: 60°C.

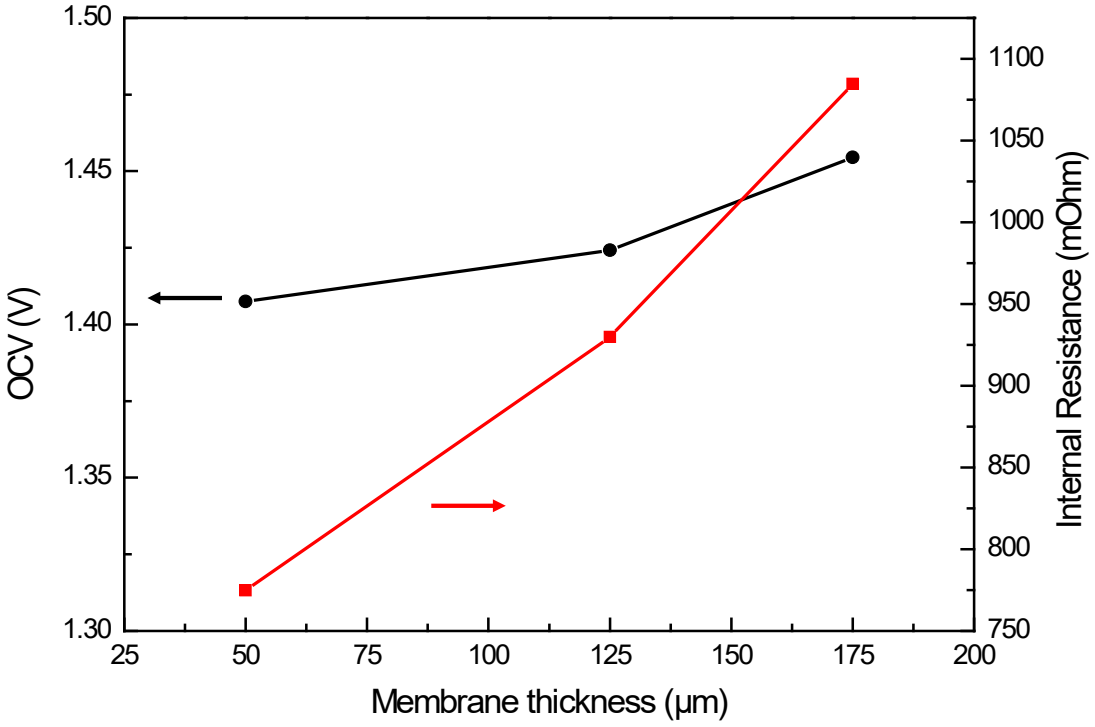

Figure 9 (b) Effect of the membrane thickness on the internal resistance. Anode: 1.0 M EG and 7.0 M NaOH aqueous solution, 2.0 mL min^{-1}. Cathode: 1.0 M H_2SO_4 and 4.0 M H_2O_2 aqueous solution, 2.0 mL min^{-1}. Temperature: 60°C.

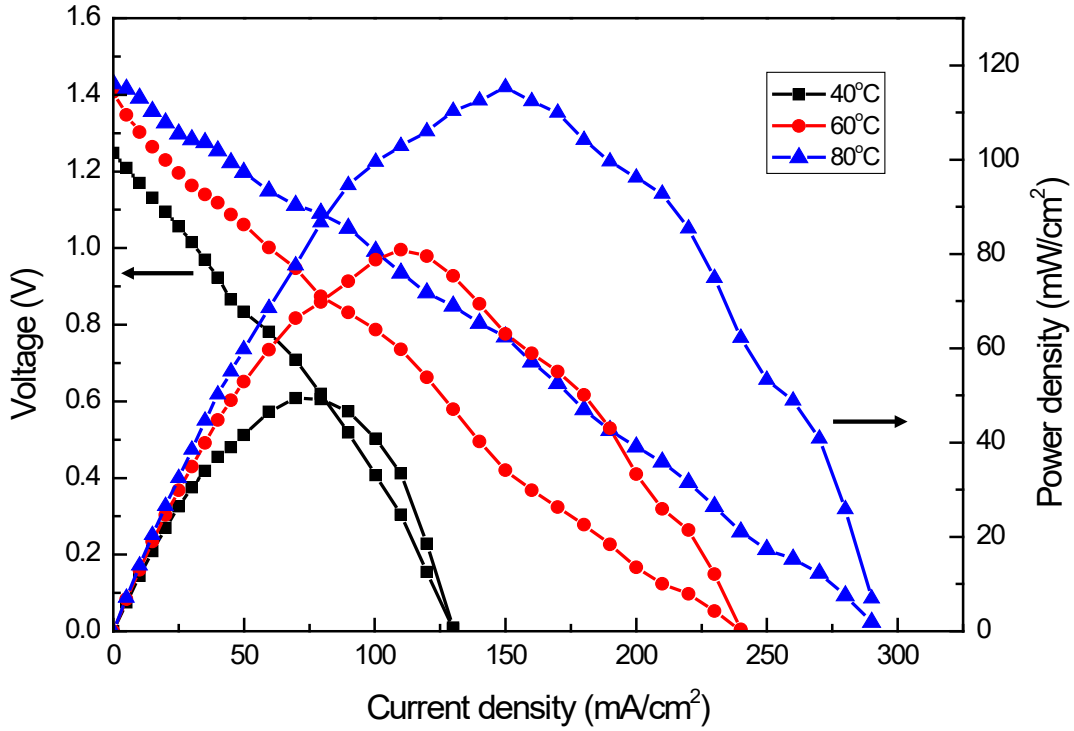

Figure 10 Effect of the temperature on the cell performance. Anode: 1.0 M EG and 7.0 M NaOH aqueous solution, 2.0 mL min^{-1}. Cathode: 1.0 M H_2SO_4 and 4.0 M H_2O_2 aqueous solution, 2.0 mL min^{-1}. Membrane: Nafion 212.